




# PTEN regulates proliferation and osteogenesis of dental pulp cells and adipogenesis of human adipose-derived stem cells

Nunthawan Nowwarote<sup>1,2,3</sup>  | Thanaphum Osathanon<sup>1</sup> | Benjamin P.J. Fournier<sup>2,3</sup> |  
 Thanakorn Theerapanon<sup>4</sup>  | Somchai Yodsanga<sup>5</sup> | Paksinee Kamolratanakul<sup>6</sup> |  
 Thantrira Porntaveetus<sup>4</sup>  | Vorasuk Shotelersuk<sup>7,8</sup>

<sup>1</sup>Dental Stem Cell Biology Research Unit and Department of Anatomy, Faculty of Dentistry, Chulalongkorn University, Bangkok, Thailand

<sup>2</sup>Centre de Recherche des Cordeliers, Université de Paris, Sorbonne Université, Paris, France

<sup>3</sup>Dental Faculty Garanciere, Oral Biology Department, Université de Paris, Paris, France

<sup>4</sup>Genomics and Precision Dentistry Research Unit and Department of Physiology, Faculty of Dentistry, Chulalongkorn University, Bangkok, Thailand

<sup>5</sup>Department of Oral Pathology, Faculty of Dentistry, Chulalongkorn University, Bangkok, Thailand

<sup>6</sup>Department of Oral and Maxillofacial Surgery, Faculty of Dentistry, Chulalongkorn University, Bangkok, Thailand

<sup>7</sup>Center of Excellence for Medical Genomics, Medical Genomics Cluster, Department of Pediatrics, Faculty of Medicine, Chulalongkorn University, Bangkok, Thailand

<sup>8</sup>Excellence Center for Genomics and Precision Medicine, King Chulalongkorn Memorial Hospital, The Thai Red Cross Society, Bangkok, Thailand

## Correspondence

Thantrira Porntaveetus, Genomics and Precision Dentistry Research Unit, Department of Physiology, Faculty of Dentistry, Chulalongkorn University, Bangkok, Thailand.  
 Email: thantrira.p@chula.ac.th

## Funding information

National Research Council of Thailand, TSRI Fund, Grant/Award Number: CU\_FRB640001\_01\_32\_3, CU\_FRB640001\_01\_32\_4 and CU\_FRB640001\_01\_30\_10; Thailand Research Fund, Grant/Award Number: RSA6180019, MRG6280001 and DPG6180001; Ratchadapiseksompot Endowment Fund (2021), Chulalongkorn University, Grant/Award Number: 764002-HE01

## Abstract

**Objective:** To investigate the role of phosphatase and tensin homolog (PTEN) in dental pulp cells (hDPs) and adipose-derived mesenchymal stem cells (hADSCs).

**Materials and Methods:** Genetic variant was identified with exome sequencing. The hDPs isolated from a patient with Cowden syndrome were investigated for their proliferation, osteogenesis, adipogenesis, and gene expression compared with controls. The normal hDPs and hADSCs were treated with the PTEN inhibitor, VO-OHpic trihydrate (VOT), to investigate the effect of PTEN inhibition.

**Results:** A heterozygous nonsense *PTEN* variant, c.289C>T (p.Gln97\*), was identified in the Cowden patient's blood and intraoral lipomas. The mutated hDPs showed significantly decreased proliferation, but significantly upregulated *RUNX2* and *OSX* expression and mineralization, indicating enhanced osteogenic ability in mutated cells. The normal hDPs treated with VOT showed the decreases in proliferation, colony formation, osteogenic marker genes, alkaline phosphatase activity, and mineral deposition, suggesting that PTEN inhibition diminishes proliferation and osteogenic potential of hDPs. Regarding adipogenesis, the VOT-treated hADSCs showed a reduced number of cells containing lipid droplets, suggesting that PTEN inhibition might compromise adipogenic ability of hADSCs.

**Conclusions:** PTEN regulates proliferation, enhances osteogenesis of hDPs, and induces adipogenesis of hADSCs. The gain-of-function *PTEN* variant, p.Gln97\*, enhances osteogenic ability of PTEN in hDPs.

## KEYWORDS

cancer, hamartoma, lipoma, metastasis, oncogene

## 1 | INTRODUCTION

Phosphatase and tensin homolog (*PTEN*, OMIM \*601728) is a tumor suppressor gene that controls several cell functions, proliferation, and differentiation. *PTEN* encodes a dual lipid and protein phosphatase that dephosphorylates the lipid phosphatidylinositol-3,4,5-triphosphate (PIP<sub>3</sub>) to the phosphatidylinositol 4,5-bisphosphate (PIP<sub>2</sub>) (Zheng et al., 2020). Heterozygous germline mutations in the *PTEN* gene have been associated with an autosomal dominant Cowden syndrome 1 (MIM #158350/ Bannayan-Riley-Ruvalcaba syndrome/ Lhermitte-Duclos syndrome), macrocephaly/autism syndrome (MIM #605309), and increased susceptibility to meningioma (MIM #607174) (Clipperton-Allen & Page, 2020; Golas et al., 2019; Martinez-Domenech et al., 2019). Cowden syndrome 1 is characterized by macrocephaly, acral keratoses, papillomatous papules, multiple lipomas involving intraoral mucosa, hemangiomas, intellectual disability, and susceptibility for breast, gastrointestinal tract, thyroid, and endometrial cancers.

*PTEN* participates in the PI<sub>3</sub>K/AKT survival pathway activating in multiple cancers (Carnero & Paramio, 2014; Fan et al., 2019; Wang et al., 2018). The *PTEN* somatic mutation increases prostate cancer susceptibility (MIM #176807). Numerous miRNAs promote cancer initiation, growth, and metastasis via targeting *PTEN* (Fang et al., 2017; Yu et al., 2017; Zhao et al., 2019). *PTEN* also regulates stem cells. *PTEN* knockdown promotes neural differentiation and neurite outgrowth in neural stem cells (Lyu et al., 2015; Shen et al., 2020). *PTEN* inhibition by miR-19a/b potentially stimulates fibroblast reprogramming to the induced pluripotent stem cells (He et al., 2014). Increased cell proliferation and suppressed cell differentiation are observed in *PTEN* knockdown human embryonic stem cells (Alva et al., 2011). These evidences implicate the important role of *PTEN* in various biological processes.

Tissue or organ function of *PTEN* was investigated. The *Pten* knockout *Col2a1* expressing cells exhibited increased bone mass and cortical thickness, inferring the *PTEN* function in bone formation (Hsieh et al., 2009). In tooth development, *PTEN* was expression in dental papilla, outer enamel epithelium, stellate reticulum, and cervical loops of developing human tooth germs, suggesting that *PTEN* is involved in tooth development (Kero et al., 2016). *PTEN* overexpression attenuated periodontal inflammation in mice by modulating inflammatory cytokines (Fu et al., 2019). *PTEN* knockdown by shRNA or inhibition by the *PTEN* inhibitor, bisperoxovanadium (bpV(pic)), activated AKT and increased adipogenesis, but decreased osteogenesis in mesenchymal stem cells derived from human exfoliated deciduous teeth. *PTEN* was shown to be responsible for lineage commitment and tumorigenesis in dental pulp cells of deciduous teeth (Shen et al., 2019). However, studies of dental pulp cells isolated from the permanent teeth (hDPs) of a Cowden patient with *PTEN* variant have never been reported. The deciduous and permanent teeth exhibit different developmental processes, morphologies, histological characteristics, and genetic profiles. There are numerous genes that are differentially expressed in dental pulp cells from deciduous and permanent teeth, for example, genes involved in

cell proliferation, self-renewal, and stemness such as *HMG2*, *CDK4*, and *CDC2A* are differently expressed in favor of deciduous pulp cells (Kang et al., 2016; Kaukua et al., 2015; Kim et al., 2014). Therefore, the same gene in the cells of deciduous and permanent teeth could function differently. We therefore aim to explore the roles of *PTEN* in dental pulp cells of permanent teeth.

Mice with conditional loss of *PTEN* led to lipoma formation, presumably caused by the differentiation of preadipocytes into adipocytes forming the lipoma (Hsieh et al., 2009). *PTEN* pathogenic variants causing Cowden syndrome are associated with lipoma development. Preadipocytes obtained from a patient carrying a heterozygous *PTEN* deletion showed reduced *PTEN* protein levels, activated PI3K/AKT signaling pathway, and enhanced capacity for adipose differentiation during long-term culture (Kässner et al., 2020). These indicate the biological roles of *PTEN* in preadipocytes and adipose homeostasis, but the effects of *PTEN* on the adipogenesis of hADSCs remain unclear. The present study therefore aimed to investigate the influence of *PTEN* on the human dental pulp cells (hDPs) by studying (1) the hDPs obtained from a Cowden syndrome patient with a *PTEN* nonsense mutation and (2) the effects of the *PTEN* inhibitor treatment on the hDPs obtained from healthy individuals. The application of *PTEN* inhibitor in hADSCs was also investigated to expand an understanding of *PTEN* involvement in adipogenesis.

## 2 | MATERIALS AND METHODS

This study was approved by the Human Research Ethic Committee, Faculty of Dentistry (No.079/2018), Faculty of Medicine, Chulalongkorn University (No.264–62), and performed according to the ethical standards of the 1964 Declaration of Helsinki and its amendments. Written informed consents were obtained from all participants.

### 2.1 | Exome Sequencing and Sanger sequencing

A patient with Cowden syndrome and his mother were recruited. Peripheral blood leukocytes obtained from the patient and his mother, and an intraoral lipoma from the patient were extracted for genomic DNA and sent to MacroGen Inc. (Seoul, Korea) for exome sequencing using Illumina HiSeq4000 sequencer. The variant analysis was performed as previously described (Intarak et al., 2018; Pornraveetus et al., 2017). Pathogenic variants were identified if they (1) passed all quality filters during variants calling process, (2) had total read depth >10, (3) were located in the coding regions and canonical splice sites of genes related to lipomatous tumor according to the Human Phenotype Ontology (HP:0012031) (Köhler et al., 2018), (4) had <1% minor allele frequency in the Genome Aggregation Database (gnomAD), Exome Variant Server, 1000 Genomes Project Consortium, dbSNPs, and in-house database of 3,206 Thai exomes, and (5) classified as pathogenic or

likely pathogenic according to the ACMG standards and guidelines (Richards et al., 2015). The identified variant was confirmed by Sanger sequencing using primers, F: GGGGAAAATAATACCTGGCTTCCT and R: TCTCTGGTCCTTACTTCCCAT.

## 2.2 | Cell characterization and behavior

Human dental pulp cells (hDPs) were isolated from the patient's third molar. Healthy dental pulp cells (controls) were obtained from the third molars of age-matched healthy individuals ( $18 \pm 1$  years of age). For adipose tissue derived cells, adipose tissues were obtained from waste tissues during surgical procedure for iliac bone graft harvesting and incubated with collagenase solution (Sigma-Aldrich, Missouri, USA). Cells were maintained in growth medium (Dulbecco's modified eagle medium (DMEM) (Gibco, MA, USA) supplemented with 10% feta bovine serum, 100 U/mL penicillin, 2 mM L-glutamine, 250 ng/mL amphotericin B, and 100  $\mu$ g/mL streptomycin) in 100% humidity with 5% carbon dioxide at 37°C. Cells at passage 3–7 were used for experiments.

## 2.3 | Osteogenic and adipogenic differentiations

For osteogenic differentiation, cells were maintained in growth medium supplemented with  $\beta$ -glycerophosphate (5 mM), L-ascorbic acid (50  $\mu$ g/mL), and dexamethasone (100 nM). Adipogenic induction medium was growth medium supplemented with insulin (1  $\mu$ g/mL), dexamethasone (1  $\mu$ M), indomethasin (100  $\mu$ M), and 3-isobutyl-1-methylxanthine (500  $\mu$ M). In some experimental conditions, culture medium was supplemented with PTEN inhibitor, VO-OHpic trihydrate (VOT) (C12H17N2O10V) (Sigma-Aldrich, Missouri, USA).

## 2.4 | Flow cytometry analysis

Mesenchymal surface marker expression was evaluated using flow cytometry analysis. The fluorescence-conjugated primary antibodies used in the cocktail were PerCP-conjugated anti-CD45 (Immuno Tools, Friesoythe, Germany), FITC conjugated anti-human CD44 (BD Bioscience Pharmingen, NJ, USA), APC-conjugated anti-human CD90 (Immuno Tools), and PE-conjugated anti-human CD105 (Immuno Tools). Samples were analyzed using a FACS<sup>Calibur</sup> Flow cytometer (BD Bioscience, CA, USA). For cell cycle analysis, cells in suspension were stained with PI/RNase staining buffer (Sigma, USA) for 30 mins at room temperature and subsequently analyzed with FACS<sup>Calibur</sup> Flow cytometer.

## 2.5 | Cell proliferation assay

Cell proliferation was evaluated using MTT (3-(4,5-dimethylthiazol-2-yl)-2,5-diphenyl tetrazolium bromide) assay. Briefly, cells were

incubated with 0.5 mg/mL MTT solution for 15 mins at 37°C. The precipitated formazan crystals were solubilized with the mixture of dimethylsulfoxide and glycine buffer. The solution was measured an absorbance at 570 nm. The percentage of cell number was calculated.

## 2.6 | Colony-forming unit assay

Cells were seeded in 6-well tissue culture plates at density of 500 cells/well and maintained in growth medium for 14 days. Fresh medium was replaced every 2 days. At Day 14, cells were stained with Coomassie blue staining.

## 2.7 | Real-time polymerase chain reaction

Total cellular RNA was collected using TRIzol reagent (RiboEx<sup>TM</sup>, GeneAll<sup>®</sup> Seoul, Korea). RNA quality and quantity were determined using nanodrop. 1  $\mu$ g of total RNA was converted to complimentary DNA using a reverse transcriptase kit (Promega, WI, USA). One microliter of complimentary DNA was employed in polymerase chain reaction with FastStart<sup>®</sup> Essential DNA Green Master (Roche, Germany). The polymerase chain reaction and melting curve analysis was performed in a CFX Connect<sup>TM</sup> Real-Time PCR (Bio-rad, USA). The oligonucleotide sequences were shown in Table S1. The expression levels of target genes were normalized to the expression levels of 18S and further normalized to the control.

## 2.8 | Immunofluorescence staining of collagen

Cells were stained with primary antibody (mouse monoclonal IgG anti Collagen 1, Abcam, USA) at dilution 1:250 for 18 h., followed by goat anti-mouse secondary antibody (Invitrogen, USA) at dilution 1:500 and streptavidin-FITC (Sigma-Aldrich, USA) at dilution 1:1,000. The nuclei were counterstained with DAPI solution. The images were captured by the fluorescence microscope (Apotome.2 Zeiss Observer.Z1, Germany). The negative control was performed by omitting primary antibody incubation.

## 2.9 | Alkaline phosphatase staining

Cells were fixed with 10% buffered formalin for 10 mins and gently washed twice with phosphate-buffered saline. ALP staining was performed using NBT/BCIP Ready-to-Use Tablets (Roche, Germany). Images were captured with Microscope ECLIPSE Ts2, Nikon-DS-Fi3 (Japan).

## 2.10 | Alizarin red staining

Samples were stained with 1% w/v alizarin red s (Sigma-Aldrich) solution at room temperature for 3 mins. Images were captured with

Microscope ECLIPSE Ts2, Nikon-DS-Fi3 (Japan). For quantitative analysis, samples were destained with 10% cetylpyridium chloride monohydrate in 10 mM sodium phosphate (Sigma-Aldrich). The absorbance of solution was measured with microplate reader (Biotek ELX800, USA) at 570 nm.

## 2.11 | Statistical analysis

Data were presented as mean  $\pm$  standard error of mean. Each dot represented the individual value. Biological replications were performed. Graph plotting and statistical analyses were performed by Prism GraphPad version 8.3.1 (GraphPad Software, USA). Mann-Whitney U test was utilized for two group comparison, and Kruskal-Wallis test following by pairwise comparison was employed for three or more group comparison. The statistically significant difference was considered when  $p < 0.05$ .

## 3 | RESULTS

### 3.1 | Patient phenotype

The patient was an 18-year-old Thai male. He was born at term with a birth weight of 3,200 g. Pregnancy was unremarkable. At 1 year of age, he developed lipomas on his back and dorsum of right foot which were getting larger and were surgically removed. At 6 years of age, the patient presented with fatty infiltrate mass at the right anterior abdominal wall. Computerized tomographic scan revealed a well-defined homogeneous fat attenuation lesion extending from lower T1 level to the pelvic brim and diffuse fat infiltrative lesion at right posterior pararenal space, small bowel, mesentery, bilateral lower abdomen, and pelvic area which caused displacement of the small bowel, ascending and descending colon, and superior mesenteric vessels. Fat infiltration was also detected in the right external oblique and right gluteus muscles. Liver, gall bladder, pancreas, spleen, adrenal glands, and kidneys appeared normal. No bony involvement was noticed. His complete blood count, blood urea nitrogen, creatinine, lipid profile, prothrombin time, and partial thromboplastin time were within normal limits.

At 18 years of age, he had intellectual disability and chronic severe pain. Physical examination showed macrocephaly, large and malformed right foot, macrodactyly of the right fifth finger, and leg length discrepancy (Figure 1a-g). Lipomas were observed on his back around costovertebral area, abdomen, inguinal area, right and left thighs, and right foot.

Radiographs showed enlarged size of right leg with increased thickness of intermuscular and subcutaneous fat at posterior aspect, enlargement of the right foot and the first and second toes with infiltrative soft tissue mass and multiple phleboliths at medial and dorsal aspects of right foot, and soft tissue swelling with tortuous density surrounding proximal phalanx of right little finger and bone erosion at the volar cortex, mild scoliosis of thoracolumbar spine convex to the left side, protruded forehead, and skeletal class III malocclusion with retrognathic maxilla and orthognathic mandible (Figure 1h-n).

His mother noticed that the patient had swollen cheek and tooth pain. The patient was then referred for dental treatment. Oral examination revealed right cheek and buccal mucosa swelling, impacted lower right third molar with large dental cavity, multiple tooth caries, heavy plaque and calculus, inflamed gingiva, and multiple soft tissue masses at the left lateral side of tongue. Dental radiographs revealed four impacted third molars and multiple proximal caries. The lower right third molar, lower right second molar, and upper second molars had large cavities (Figure 1o-r). The dental treatment was carried out under general anesthesia. Four third molars were surgically removed. Two upper second molars and lower right second molar, diagnosed with irreversible pulpitis, were extracted. Biopsy of the soft tissue mass showed a mass of fibro-fatty connective tissue covered by parakeratinized stratified squamous epithelium, decreased rete ridges, various bundles of muscle fibers beneath the epithelium, and numerous mature adipocytes in the stroma, indicating the lipoma (Figure 1r-t). Other members of the family are unaffected.

### 3.2 | Variant analysis

Exome sequencing identified a heterozygous nonsense variant c.289C>T (p. Gln97\*) in the exon 5 of the *PTEN* gene (NM\_000314.8) in the patient's blood and intraoral lipoma. The variant was classified as pathogenic based on the ACMG standards and guidelines (Richards et al., 2015) and previously reported in a patient with Cowden syndrome (Nelen et al., 1999). Sanger sequencing confirmed that the *PTEN* variant was detected in the patient's blood and lipoma but not in his mother (Supplementary Figure 1). The patient was diagnosed with Cowden syndrome 1 (MIM #158350).

### 3.3 | *PTEN*-mutated hDPs show reduced cell proliferation, but increased osteogenesis

Cells isolated from dental pulp tissues of the *PTEN*-mutated patient were positive for CD44, CD90, and CD105 expression (Figure 2(a))

**FIGURE 1** Patient's characteristics. (a-g) The patient presented with macrocephaly, large and malformed right foot, and macrodactyly of the right fifth finger. (h-n) Radiographs showed mild scoliosis of thoracolumbar spine convex to the left side, enlarged size of right leg, right foot, and the first and second toe, soft tissue swelling surrounding proximal phalanx of right little finger and bone erosion at the volar cortex, protruded forehead, retrognathic maxilla, and orthognathic mandible. (o-q) Dental radiographs showed four impacted third molars and multiple caries. (r) Lipomas were observed on the left lateral side of tongue. (s, t) Biopsy showed a mass of fibro-fatty connective tissue covered by parakeratinized stratified squamous epithelium, various bundles of muscle fibers beneath the epithelium, and numerous mature adipocytes in the stroma, indicating the lipoma.



but negative for CD45 expression (data not shown), indicating mesenchymal cells. These observations were consistent with those cells isolated from healthy donors (Figure 2a). The hDPs from both *PTEN*-mutated and healthy donors were able to proliferate in vitro (Figure 2b). The significant increases in cell numbers were observed at Days 3 and 7 compared with Day 1 in *PTEN*-mutated hDPs and two controls. However, it was noted that the cell numbers of *PTEN*-mutated hDPs at Days 3 and 7 were significantly lower than those of two controls.

The osteogenic marker gene expression and the in vitro mineralization were examined using real-time PCR and alizarin red s staining, respectively. On Day 7 compared with Day 3 after osteogenic induction, *PTEN*-mutated hDPs showed markedly increased *RUNX2* and *OSX* mRNA expression 3.6- and 6.7-folds, respectively; on the contrary, the mRNA levels of these two genes were decreased in Donors 1 and 2 (Figure 2c, d). Correspondingly, a dramatic increase in mineral deposition was observed in *PTEN*-mutated hDPs compared with those of Donors 1 and 2 at 14 days after osteogenic induction (Figure 2e, f).

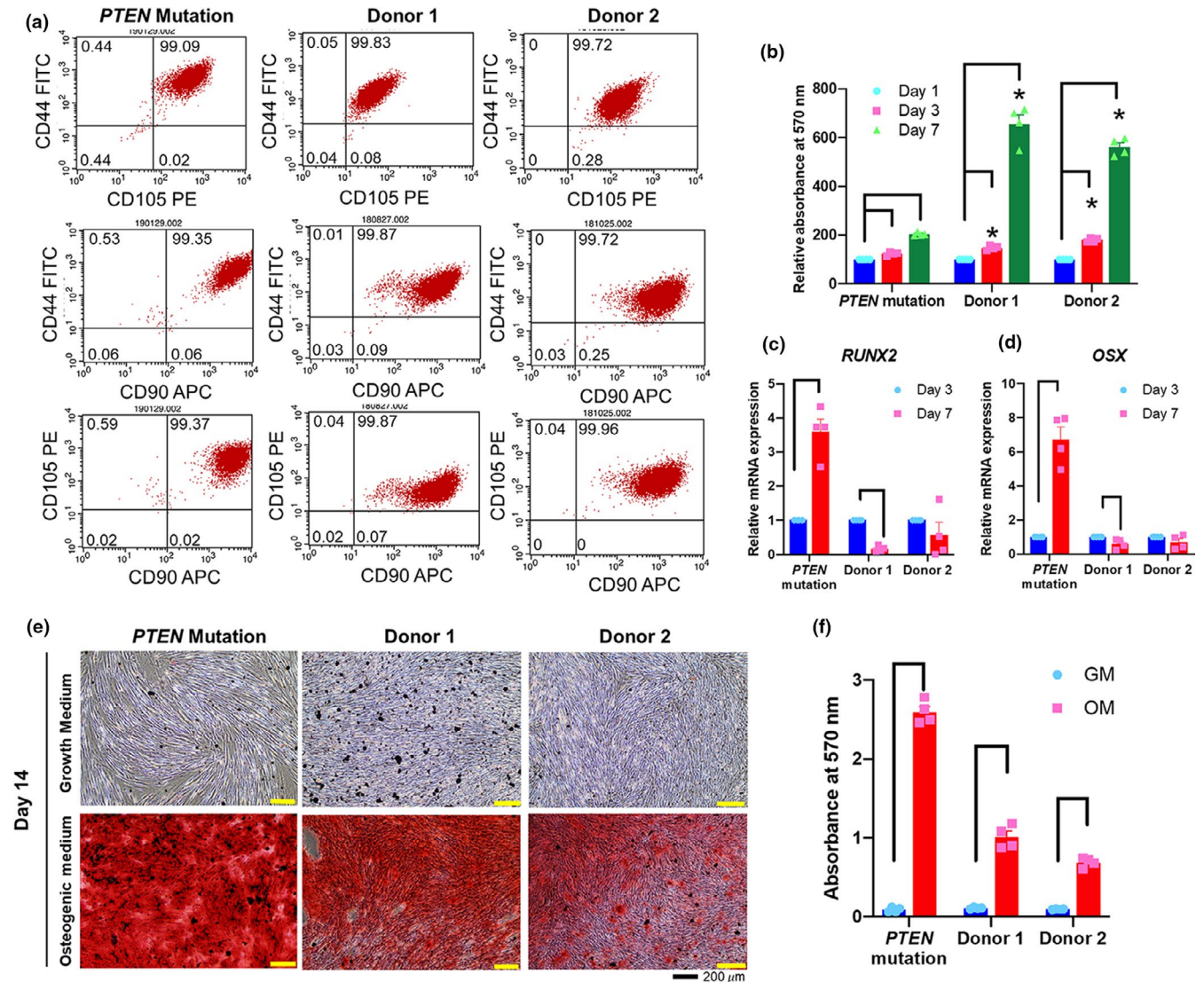


**FIGURE 2** Characterization of cells isolated from dental pulp tissues of a patient with Cowden syndrome and *PTEN* mutation. (a) The expression of mesenchymal stem cell markers, CD44, CD90, and CD105 was examined using flow cytometry. (b) Cells were maintained in normal growth medium, and cell viability was tested at Day 1, 3, and 7 using MTT assay. (c-d) Cells were maintained in osteogenic induction medium (OM) for 7 days, and the mRNA expression of osteogenic marker genes, *RUNX2* and *OSX*, was determined using real-time PCR. (e) Cells were maintained in osteogenic induction medium for 14 days. The mineral deposition was determined using alizarin red s staining. (f) The absorbance of the solubilized alizarin red s dye was measured at 570 nm. Cells maintained in the normal growth medium (GM) were used for comparison. Cells isolated from dental pulp tissues of healthy subjects were employed as controls (donor 1 and 2). Bars indicate the statistically significant difference within the same sample at difference situations. Asterisks indicate the statistically significant difference between *PTEN*-mutated cells and donor 1 or donor 2 at the same time point.

### 3.4 | PTEN inhibition by VOT reduces colony formation and osteogenesis, but not adipogenesis of wild-type hDPs

To examine the effect of PTEN inhibition on wild-type hDPs behaviors, hDPs from healthy donors were treated with VO-OHpic trihydrate (VOT), a PTEN inhibitor. The hDPs were exposed with VOT at the concentration of 0.625 to 5  $\mu$ M and maintained in normal growth medium. Cell viability was examined using MTT assay at Days 1, 3, and 7 (Figure 3a). At Day 1, there was no significant difference of cell viability in all VOT-treated concentration. At Day 3, hDPs exposed to the higher doses of VOT demonstrated a slightly more reduction of cell numbers. At Day 7 compared to Day 3, the differences of the cell proliferation were more obvious, with the more concentration of VOT, the lower the cell proliferation. The 5  $\mu$ M VOT abolished colony formation at Day 14 (Figure 3b). Further, cell cycle analysis at 72 h after VOT (5  $\mu$ M) treatment demonstrated the slight decrease of population in S phase and the increase in population in G2/M phase (Figure 3c, d).

In osteogenic condition, the *COL1* and *ALP* expression was suppressed in VOT (5  $\mu$ M) treated condition at Day 7 (Figure 3e-j). Similarly, an in vitro mineral deposition was markedly reduced in cells exposed to VOT for 14 days (Figure 3k, l). This was confirmed by the significant reduction of absorbance of solubilized alizarin red s staining (Figure 3m). In addition, the significant decreases of osteogenic marker gene expression comprising *RUNX2*, *ALP*, *COL1A1*, and *OCN* were observed in cells treated with VOT after maintaining in osteogenic induction medium for 7 days (Figure 3n-r). In addition, we investigated the expression of adipogenic marker genes in healthy hDPs in growth medium or adipogenic medium with and without VOT treatment. The *LPL* and *PPAR $\gamma$*  expression in VOT-treated hDPs was not significantly different from untreated hDPs (Figure 3s, t).

Here, we reported that *PTEN*-mutated hDPs exhibited higher osteogenic potency compared with cells from healthy donors while PTEN inhibitor suppressed osteogenic differentiation in wild-type hDPs. These results may imply that this nonsense *PTEN* mutation, c.289C>T (p. Gln97\*), enhances osteogenic ability of PTEN in hDPs.

### 3.5 | PTEN inhibition attenuates adipogenic differentiation in hADSCs

Multiple lipomas are one of the typical features found in *PTEN*-mutated patients. Exome sequencing also detected the *PTEN* mutation, c.289C>T (p. Gln97\*), in the proband's lipoma. We thus further investigate the role of *PTEN* in adipogenesis using PTEN inhibitor and hADSCs. The hADSCs were cultured in adipogenic induction medium in the presence or absence of VOT (5  $\mu$ M). Intracellular lipid accumulation was observed under light microscope. Oil red O staining and phase contrast microscopy showed that the number of cells containing lipid droplets in VOT-treated adipogenic medium was fewer than that in untreated adipogenic medium at Day 16 (Figure 4a-i). In addition, the expression of adipogenic markers, *LPL* and *PPAR $\gamma$* ,

was attenuated in the VOT-treated condition at Day 8 (Figure 4g, h), although the difference was not statistically significant. We also observed a slight increase in *PTEN* mRNA in hADSCs cultured in adipogenic medium (Figure 3i). In normal growth medium, no significant difference in cell number was observed in hADSCs treated with VOT compared with the untreated controls at Day 7 (Supplementary Figure 2).

## 4 | DISCUSSION

PTEN has been previously shown to have various effects on different cell types. The PTEN inhibitor VO-OHpic was proved to be a highly potent inhibitor of PTEN (Mak et al., 2010). Many studies have demonstrated the efficiency of VO-OHpic in PTEN inhibition, which results in the elevated levels of PI3K and P-AKT in multiple cell types including tendon stem cells (Wang et al., 2019), nucleus pulposus cells (Qin et al., 2020), bladder carcinoma cell (Lin et al., 2019), and human dental pulp cells derived from the deciduous teeth (Shen et al., 2019). These evidences suggest that the VO-OHpic is an efficient PTEN inhibitor in various cells. VOT reduced the proliferation of Hep3B and PLC/PRF/5 cell lines (Augello et al., 2016) and human breast cancer cells (Yang et al., 2017). In contrast, increased proliferation was reported in osteosarcoma cells treated with VOT (Xi & Chen, 2017) and in genetically knockout of *PTEN* in rabbit bone marrow-derived mesenchymal stem cells (Shen et al., 2018). These suggest that the inhibition of PTEN on cell proliferation is cell type-dependent. The present study demonstrated that the PTEN inhibition by VOT led to a marked decrease in cell proliferation and colony-forming unit of human dental pulp cells (hDPs) in a dose dependent manner, suggesting that PTEN increases proliferation of hDPs. In addition, PTEN has been shown to control cell cycle progression (Brandmaier et al., 2017). We observed the slightly increased percentage of hDPs in G2/M subpopulation when treated with VOT compared with untreated. Corresponding to a previous report, VOT-treated Hep3B cells exhibited an increase in G2/M population compared with controls (Augello et al., 2016). These suggest that PTEN is involved in cell proliferation and cell cycle.

Regarding osteogenesis, we reported that PTEN inhibition with VOT attenuated osteogenic potency of hDPs as shown by the reductions in *COL1* expression, ALP enzymatic activity, mineral deposition, and osteogenic marker gene expression. Correspondingly, CRISPR/Cas9-mediated *PTEN* knockdown in rabbit bone marrow derived mesenchymal stem cells showed lower *Runx2* mRNA expression and mineral deposition (Shen et al., 2018). Similarly, VOT treatment suppressed an in vitro mineral deposition and expression of *Alp* and *Runx2* mRNA in mouse embryonic palatal mesenchymal cells after osteogenic induction for 3 weeks (Shi et al., 2019). Further, PTEN inhibition by VOT treatment or shPTEN transduction in SHEDs resulted in a reduction in mineralization while PTEN overexpression led to an increase in mineral deposition and osteogenic marker gene expression (*RUNX2*, *OCN*, and *DSP*) (Shen et al., 2019). It was also shown that miR-363-3p attenuated *OCN*, *ALP*, and *COL1A1* mRNA

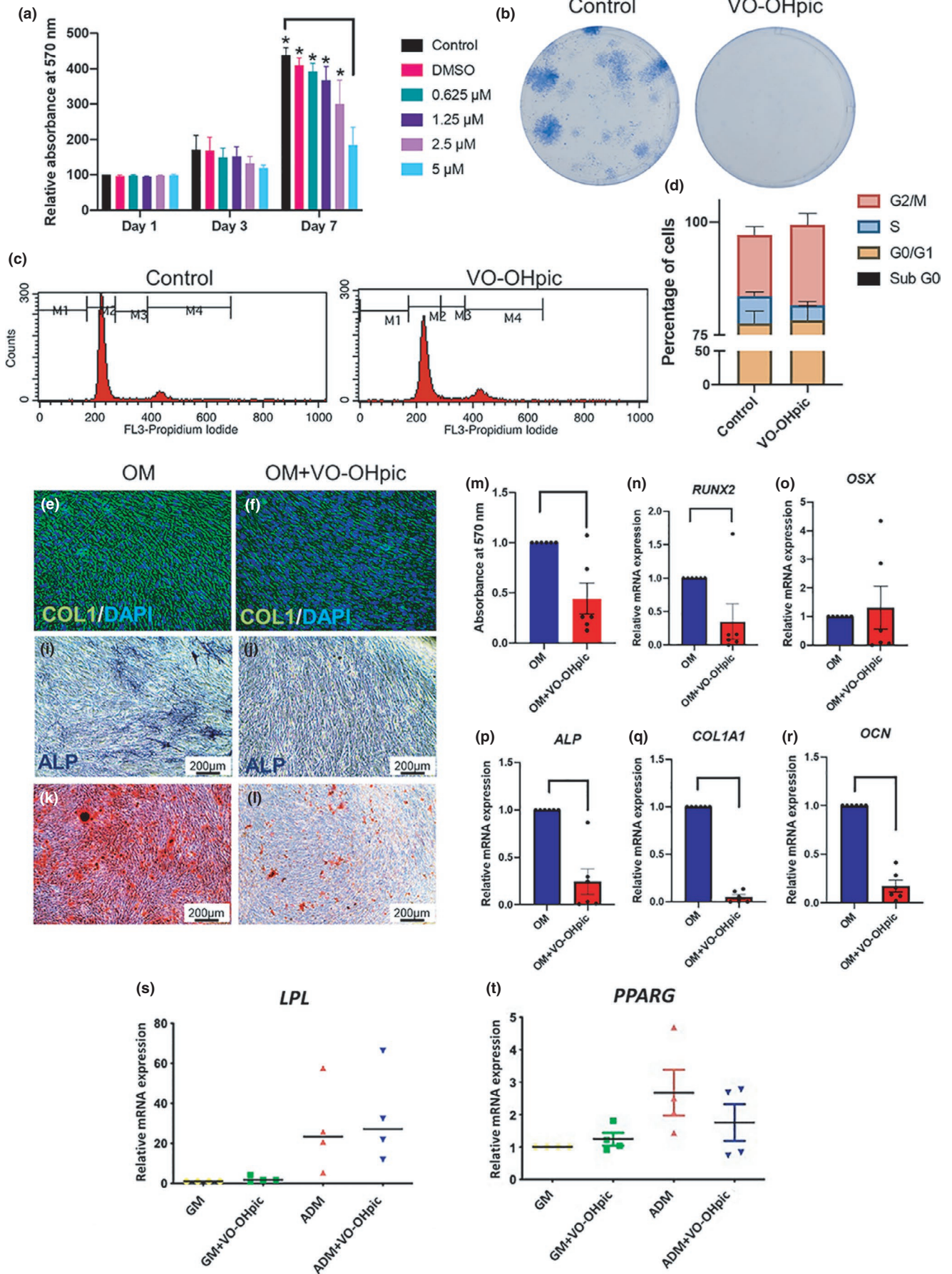




**FIGURE 3** Effects of VOT, a PTEN inhibitor, on hDPs. (a) Cells were exposed to various concentration of PTEN inhibitor VO-OHpic trihydrate, and cell viability was performed at Day 1, 3, and 7. Bars indicate the statistically significant difference between different concentrations of VO-OHpic trihydrate at Day 7. Asterisks indicate the statistically significant difference between Day 7 and Day 1 at the same concentration. (b) Colony-forming unit ability was determined at Day 14. Cell colonies were stained with Coomassie blue. (c) Cells were treated with VO-OHpic trihydrate for 72 h. Cell cycle analysis was examined using flow cytometry analysis. M1; Sub G0, M2; G0/G1, M3; S, M4; G2/M. (d) The percentages of each subpopulation in different cell cycle stages were demonstrated. Cells were maintained in osteogenic induction medium in the presence or absence of VO-OHpic trihydrate. (e-f) Immunofluorescence staining of COL1 and (i-j) ALP staining was performed at Day 7 after induction. (k-l) The in vitro mineral deposition was examined using alizarin red s staining at Day 14. (m) The relative absorbance of solubilized alizarin red s dye was demonstrated. (n-r) The osteogenic marker gene expression was determined using real-time PCR at Day 7. (s, t) The adipogenic marker gene expression was determined at Day 8 in both normal growth medium or adipogenic medium in the presence or absence of VO-OHpic trihydrate. Bars indicate the statistically significant difference. OM; osteogenic induction medium, ADM; adipogenic induction medium.

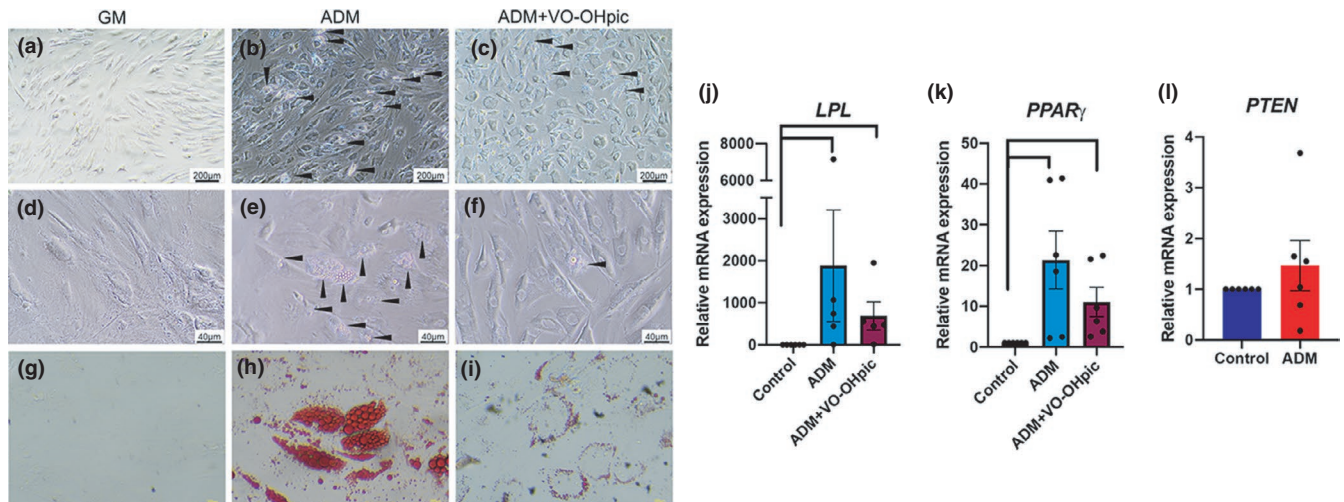


**FIGURE 4** Effects of a PTEN inhibitor on adipogenic differentiation of hADSCs. (a-f) The hADSCs were maintained in adipogenic induction medium for 16 days in the presence or absence of VO-OHpic trihydrate. Intracellular lipid accumulation was observed under phase contrast microscope. Black arrow heads indicate lipid accumulation. (g-i) Oil red O staining showed the presence of lipid droplets in cells (colored red). (j-l) The mRNA levels of adipogenic marker genes were investigated using real-time PCR at Day 8 after adipogenic induction. Bars indicate the statistically significant difference. (i) hADSCs were maintained in adipogenic medium for 8 days. *PTEN* mRNA levels were determined using real-time PCR. ADM; adipogenic induction medium.

expression in C2C12 cells via targeting PTEN (Li et al., 2019). In murine osteosarcoma cell line with Rank deletion (MOTO-Rank $\Delta/\Delta^{OC}$  cells), VOT treatment slightly decreased *Alp*, *Runx2*, *Col1a1*, and *Bsp* mRNA levels compared with the controls (Xi & Chen, 2017). These evidences confirm that PTEN acts as a positive regulator in osteogenesis.

On the other hands, PTEN also plays a role as a negative regulator in osteogenic differentiation. In this regard, miR-19b-3p was reported to reduce *PTEN* expression, but increase osteogenic differentiation potency determined by mineral deposition, alkaline phosphatase enzymatic activity, and osteogenic marker protein expression (Zhu et al., 2019). Conditional knockout *Pten* in *Osx*-Cre mice showed an increase in bone formation (Filtz et al., 2015). Calvarial osteoblasts derived from *Pten* deleted mice had a slight suppression of *Bglap*, *Runx2* and *Col1a1* at 48 hours after incubated in osteogenic induction medium (Filtz et al., 2015). However, *Pten* deleted cells exhibited an in vitro increased mineralization, suggesting the potent role of PTEN in later differentiation stage of osteogenic differentiation. The discrepancy role of PTEN in osteogenesis among publications could

be due to differences in cell types and techniques to modify PTEN expression in vitro. None of the aforementioned studies involved hDPs from the permanent teeth, while oral symptoms are observed in Cowden patients. It will then be beneficial to know the impact and role of PTEN in oral mineralizing cells and stem cells.

PTEN has also been shown to regulate adipogenesis. Mice with *Pten* deletion using *Col2a1* Cre system exhibited abnormal fat accumulation, lipoma, and higher fat marrow in the femurs compared with wild types (Hsieh et al., 2009). The *Pten* deleted mice also developed lipoma tumors but at a much lower frequency and later onset than those with co-deletion of *Pten* and *Rb1* tumor suppressor gene. Mouse calvarial osteoblasts lacking *Pten*, treated with adipogenic media for 25 days, showed increased adipocyte differentiation compared with controls, but a more pronounced adipocyte differentiation was observed in cells with co-deleting *Rb1* and *Pten* (Filtz et al., 2015). In SHEDs, genetic or chemical inhibition of PTEN also increased intracellular lipid droplets and adipogenic gene expression (Shen et al., 2019). Aspirin was shown to induce *PTEN* expression in a PTEN/PI3K/AKT pathway, resulting in a decrease in adipogenic

marker gene expression and cellular lipid storage, and adipogenic differentiation in tendon stem cells (Wang et al., 2019). An addition of VOT was able to rescue aspirin-suppressed adipogenic differentiation in tendon stem cells (Wang et al., 2019) (Wang et al., 2019). The above evidence shows that reduced PTEN level promotes adipogenic differentiation, but other molecules might contribute to the role of *PTEN* in adipogenesis.

Here, the proband was found to be heterozygous for c.289C>T (p. Gln97\*) in *PTEN*. It was previously reported in a patient with Cowden syndrome (Nelen et al., 1999). According to the proband's phenotype and genotype, the diagnosis of Cowden syndrome 1 (MIM #158350) was confirmed. The hDPs cells obtained from the proband showed compromised cell proliferation but dramatically increased osteogenic differentiation potency. To confirm the role of *PTEN* in hDPs, healthy hDPs with *PTEN* inhibition showed reduced osteogenic differentiation ability. These suggest that the *PTEN* mutation, although compromises proliferation ability, can enhance osteogenic function of *PTEN* in hDPs. We hypothesize that this *PTEN* mutation activates osteogenic signal in hDPs.

*PTEN* is involved in wide spectra of cellular processes including cell survival, proliferation, and differentiation (Venniyoor, 2020). The mutated *PTEN* with decreased cell proliferation might have reduced ability for cells to grow and divide to replenish lost cells compared with healthy cells. *PTEN* activation promotes osteogenesis in dental pulp mesenchymal cells which could affect the dentin bridge formation in vital pulp therapy or reparative dentin formation. Dysregulation of *PTEN* could therefore influence dental pulp repair and regeneration.

The proband had recurrent multiple lipomas including the intra-oral ones (Figure 1r), which are one of the typical features of Cowden syndrome, suggesting that the *PTEN* nonsense mutation (p. Gln97\*) enhances tumor formation and adipogenic differentiation. This is the reason to investigate the adipogenic differentiation of stem cells. In this regard, we selected the hADSCs to represent the human adipose tissue and mimic the lipoma formation in vitro. We observed increased *PTEN* level, although not statistically significant, in hADSCs after adipogenic induction and that *PTEN* inhibition by VOT in hADSCs led to a decrease in intracellular lipid droplets, concomitant with decreased adipogenic gene expression. Supporting this finding, a previous work demonstrated that rabbit bone marrow mesenchymal stem cells with loss of *PTEN* expression exhibited a significant decrease in *Pparγ* mRNA levels and amount of lipid droplets compared with wild-type controls (Shen et al., 2018). Our results demonstrate that *PTEN* inhibition decreases adipogenesis in hADSCs and might be of benefit for treating the lipomas in *PTEN*-mutated patients. However, more studies are required to confirm this finding. The mutated hADSCs should be further investigated.

To conclude, the present study demonstrates that *PTEN* mediates proliferation and induces osteogenic differentiation of hDPs, and induces adipogenesis of hADSCs. In a Cowden patient, the *PTEN* mutation enhances osteogenesis in hDPs. We also show that the *PTEN* mutation is detected in the intraoral lipoma of a Cowden patient and *PTEN* inhibition led to decreased adipogenesis in

hADSCs. This might be applicable for treating lipomas in Cowden patients. Lastly, we believe that the new findings of *PTEN* molecular mechanisms in osteogenesis and adipogenesis in hDPs and hADSCs would be of high value in regenerative dentistry and precision medicine.

## ACKNOWLEDGMENTS

This project is funded by the Health Systems Research Institute, National Research Council of Thailand, TSRI Fund (CU\_FRB640001\_01\_32\_3, CU\_FRB640001\_01\_32\_4, CU\_FRB640001\_01\_30\_10), Thailand Research Fund (RSA6180019, MRG6280001, DPG6180001), and Ratchadapiseksompotch Endowment Fund (2021), Chulalongkorn University (764002-HE01). N.N. is supported by the Ratchadapisek Somphot Fund for Postdoctoral Fellowship, Chulalongkorn University. Authors thank Mr. Noppadol Sa-Ard-lam and Professor Rangsin Mahanonda, the Immunology Research Center for the flow cytometry analysis.

## CONFLICTS OF INTEREST

None to declare.

## AUTHOR CONTRIBUTIONS

**Nunthawan Nowwarote:** Formal analysis; Investigation; Writing-review & editing. **Thanaphum Osathanon:** Conceptualization; Data curation; Formal analysis; Writing-original draft; Writing-review & editing. **Benjamin P.J. Fournier:** Formal analysis; Writing-review & editing. **Thanakorn Theerapanon:** Formal analysis; Writing-review & editing. **Somchai Yodsanga:** Formal analysis; Writing-review & editing. **Paksinee Kamolratanakul:** Formal analysis; Writing-review & editing. **Thantrira Porntaveetus:** Conceptualization; Formal analysis; Funding acquisition; Writing-original draft; Writing-review & editing. **Vorasuk Shotelersuk:** Data curation; Writing-review & editing.

## PEER REVIEW

The peer review history for this article is available at <https://publons.com/publon/10.1111/odi.14030>.

## DATA AVAILABILITY STATEMENT

The data that support the findings of this study are available in the supplementary material of this article.

## ORCID

Nunthawan Nowwarote  <https://orcid.org/0000-0001-5315-5565>

Thanakorn Theerapanon  <https://orcid.org/0000-0001-6727-862X>

Thantrira Porntaveetus  <https://orcid.org/0000-0003-0145-9801>

## REFERENCES

- Alva, J. A., Lee, G. E., Escobar, E. E., & Pyle, A. D. (2011). Phosphatase and tensin homolog regulates the pluripotent state and lineage fate choice in human embryonic stem cells. *Stem Cells*, 29, 1952–1962. <https://doi.org/10.1002/stem.748>
- Augello, G., Puleio, R., Emma, M. R., Cusimano, A., Loria, G. R., McCubrey, J. A., Montalto, G., & Cervello, M. (2016). A *PTEN* inhibitor displays

- preclinical activity against hepatocarcinoma cells. *Cell Cycle*, 15, 573–583. <https://doi.org/10.1080/15384101.2016.1138183>
- Brandmaier, A., Hou, S. Q., & Shen, W. H. (2017). Cell cycle control by PTEN. *Journal of Molecular Biology*, 429, 2265–2277. <https://doi.org/10.1016/j.jmb.2017.06.004>
- Carnero, A., & Paramio, J. M. (2014). The PTEN/PI3K/AKT Pathway in vivo. *Cancer Mouse Models. Frontiers in Oncology*, 4, 252. <https://doi.org/10.3389/fonc.2014.00252>
- Clipperton-Allen, A. E., & Page, D. T. (2020). Connecting Genotype with behavioral phenotype in mouse models of autism associated with PTEN mutations. *Cold Spring Harbor Perspectives in Medicine*, 10, <https://doi.org/10.1101/cshperspect.a037010>
- Fan, C., Zhao, C., Wang, F., Li, S., & Wang, J. (2019). Significance of PTEN mutation in cellular process, prognosis, and drug selection in clear cell renal cell carcinoma. *Frontiers in Oncology*, 9, 357. <https://doi.org/10.3389/fonc.2019.00357>
- Fang, H., Xie, J., Zhang, M., Zhao, Z., Wan, Y., & Yao, Y. (2017). miRNA-21 promotes proliferation and invasion of triple-negative breast cancer cells through targeting PTEN. *American Journal of Translational Research*, 9, 953–961. <https://www.ncbi.nlm.nih.gov/pubmed/28386324>
- Filtz, E. A., Emery, A., Lu, H., Forster, C. L., Karasch, C., & Hallstrom, T. C. (2015). Rb1 and Pten co-deletion in osteoblast precursor cells causes rapid lipoma formation in mice. *PLoS One*, 10, e0136729. <https://doi.org/10.1371/journal.pone.0136729>
- Fu, C., Wei, Z., & Zhang, D. (2019). PTEN inhibits inflammatory bone loss in ligature-induced periodontitis via IL1 and TNF-alpha. *BioMed Research International*, 2019, 6712591. <https://doi.org/10.1155/2019/6712591>
- Golas, M. M., Auber, B., Ripperger, T., Pabst, B., Schmidt, G., Morlot, M., Diebold, U., Steinemann, D., Schlegelberger, B., & Morlot, S. (2019). Looking for the hidden mutation: Bannayan-Riley-Ruvalcaba syndrome caused by constitutional and mosaic 10q23 microdeletions involving PTEN and BMPR1A. *American Journal of Medical Genetics Part A*, 179, 1383–1389. <https://doi.org/10.1002/ajmg.a.61166>
- He, X., Cao, Y., Wang, L., Han, Y., Zhong, X., Zhou, G., Cai, Y., Zhang, H., & Gao, P. (2014). Human fibroblast reprogramming to pluripotent stem cells regulated by the miR19a/b-PTEN axis. *PLoS One*, 9, e95213. <https://doi.org/10.1371/journal.pone.0095213>
- Hsieh, S. C., Chen, N. T., & Lo, S. H. (2009). Conditional loss of PTEN leads to skeletal abnormalities and lipoma formation. *Molecular Carcinogenesis*, 48, 545–552. <https://doi.org/10.1002/mc.20491>
- Intarak, N., Theerapanon, T., Ittiwut, C., Suphapeetiporn, K., Porntaveetus, T., & Shotelersuk, V. (2018). A novel PITX2 mutation in non-syndromic orofacial anomalies. *Oral Diseases*, 24, 611–618. <https://doi.org/https://doi.org/10.1111/odi.12804>
- Kang, J., Bai, R., Liu, K., Ji, X. P., Li, Y., & Han, J. Y. (2016). Identification of significantly different modules between permanent and deciduous teeth by network and pathway analyses. *Genetics and Molecular Research*, 15, <https://doi.org/10.4238/gmr15047959>
- Kässner, F., Kirstein, A., Händel, N., Schmid, G. L., Landgraf, K., Berthold, A., & Garten, A. (2020). A new human adipocyte model with PTEN haploinsufficiency. *Adipocyte*, 9, 290–301. <https://doi.org/10.1080/21623945.2020.1785083>
- Kaukua, N., Chen, M., Guarnieri, P., Dahl, M., Lim, M. L., Yucel-Lindberg, T., & Fried, K. (2015). Molecular differences between stromal cell populations from deciduous and permanent human teeth. *Stem Cell Research & Therapy*, 6, 59. <https://doi.org/10.1186/s13287-015-0056-7>
- Kero, D., Cigic, L., Medvedec Mikic, I., Galic, T., Cubela, M., Vukojevic, K., & Saraga-Babic, M. (2016). Involvement of IGF-2, IGF-1R, IGF-2R and PTEN in development of human tooth germ - an immunohistochemical study. *Organogenesis*, 12, 152–167. <https://doi.org/10.1080/15476278.2016.1197460>
- Kim, J.-H., Jeon, M., Song, J.-S., Lee, J.-H., Choi, B.-J., Jung, H.-S., Moon, S. J., DenBesten, P. K., & Kim, S.-O. (2014). Distinctive genetic activity pattern of the human dental pulp between deciduous and permanent teeth. *PLoS One*, 9, e102893. <https://doi.org/10.1371/journal.pone.0102893>
- Köhler, S., Carmody, L., Vasilevsky, N., Jacobsen, J. O. B., Danis, D., Gouridine, J.-P., & Robinson, P. N. (2018). Expansion of the Human Phenotype Ontology (HPO) knowledge base and resources. *Nucleic Acids Research*, 47, D1018–D1027. <https://doi.org/10.1093/nar/gky1105>
- Li, M., Luo, R., Yang, W., Zhou, Z., & Li, C. (2019). miR-363-3p is activated by MYB and regulates osteoporosis pathogenesis via PTEN/PI3K/AKT signaling pathway. *In Vitro Cellular & Developmental Biology*, 55, 376–386. <https://doi.org/10.1007/s11626-019-00344-5>
- Lin, Y.-H., Tsui, K.-H., Chang, K.-S., Hou, C.-P., Feng, T.-H., & Juang, H.-H. (2019). Maspin is a PTEN-upregulated and p53-upregulated tumor suppressor gene and acts as an hdac1 inhibitor in human bladder cancer. *Cancers*, 12, 10. <https://doi.org/10.3390/cancers12010010>
- Lyu, J., Yu, X., He, L., Cheng, T., Zhou, J., Cheng, C., Chen, Z., Cheng, G., Qiu, Z., & Zhou, W. (2015). The protein phosphatase activity of PTEN is essential for regulating neural stem cell differentiation. *Molecular Brain*, 8, 26. <https://doi.org/10.1186/s13041-015-0114-1>
- Mak, L. H., Vilar, R., & Woscholski, R. (2010). Characterisation of the PTEN inhibitor VO-OHPic. *Journal of Chemical Biology*, 3, 157–163. <https://doi.org/10.1007/s12154-010-0041-7>
- Martinez-Domenech, A., Garcia-Legaz Martinez, M., Magdaleno-Tapial, J., Perez-Pastor, G., Rodriguez-Lopez, R., & Perez-Ferriols, A. (2019). Novel PTEN mutation in Cowden syndrome: case report with late diagnosis and non-malignant course. *Dermatology Online Journal*, 25, <https://www.ncbi.nlm.nih.gov/pubmed/31220904>
- Nelen, M. R., Kremer, H., Konings, I. B., Schoute, F., van Essen, A. J., Koch, R., Woods, C. G., Fryns, J. P., Hamel, B., Hoefsloot, L. H., Peeters, E. A., & Padberg, G. W. (1999). Novel PTEN mutations in patients with Cowden disease: absence of clear genotype-phenotype correlations. *European Journal of Human Genetics*, 7, 267–273. <https://doi.org/10.1038/sj.ejhg.5200289>
- Porntaveetus, T., Srichomthong, C., Suphapeetiporn, K., & Shotelersuk, V. (2017). Monoallelic FGFR3 and Biallelic ALPL mutations in a Thai girl with hypochondroplasia and hypophosphatasia. *American Journal of Medical Genetics Part A*, 173, 2747–2752. <https://doi.org/https://doi.org/10.1002/ajmg.a.38370>
- Qin, J., Fu, M., Wang, J., Huang, F., Liu, H., Huangfu, M., Yu, D., Liu, H., Li, X., Guan, X., & Chen, X. (2020). PTEN/AKT/mTOR signaling mediates anticancer effects of epigallocatechin-3-gallate in ovarian cancer. *Oncology Reports*, 1885–1896. <https://doi.org/10.3892/or.2020.7571>
- Richards, S., Aziz, N., Bale, S., Bick, D., Das, S., Gastier-Foster, J., & Rehm, H. L. (2015). Standards and guidelines for the interpretation of sequence variants: a joint consensus recommendation of the American College of Medical Genetics and Genomics and the Association for Molecular Pathology. *Genetics in Medicine*, 17, 405–423. <https://doi.org/10.1038/gim.2015.30>
- Shen, H., Wang, J., Shen, L., Wang, H., Li, W., & Ding, X. (2020). Phosphatase and tensin homolog deletion enhances neurite outgrowth during neural stem cell differentiation. *Neuropathology*, 40, 224–231. <https://doi.org/10.1111/neup.12633>
- Shen, W.-C., Lai, Y.-C., Li, L.-H., Liao, K., Lai, H.-C., Kao, S.-Y., Wang, J., Chuong, C.-M., & Hung, S.-C. (2019). Methylation and PTEN activation in dental pulp mesenchymal stem cells promotes osteogenesis and reduces oncogenesis. *Nature Communications*, 10(1), <https://doi.org/10.1038/s41467-019-10197-x>
- Shen, Y., Zhang, J., Yu, T., & Qi, C. (2018). Generation of PTEN knock-out bone marrow mesenchymal stem cell lines by CRISPR/Cas9-mediated genome editing. *Cytotechnology*, 70, 783–791. <https://doi.org/10.1007/s10616-017-0183-3>
- Shi, L., Li, B., Zhang, B., Zhen, C., Zhou, J., & Tang, S. (2019). Mouse embryonic palatal mesenchymal cells maintain stemness through the

- PTEN-Akt-mTOR autophagic pathway. *Stem Cell Research & Therapy*, 10, 217. <https://doi.org/10.1186/s13287-019-1340-8>
- Venniyoor, A. (2020). PTEN: A Thrifty Gene That Causes Disease in Times of Plenty? [Hypothesis and Theory]. *Frontiers in Nutrition*, 7, 81. <https://doi.org/10.3389/fnut.2020.00081>
- Wang, X., Cao, X., Sun, R., Tang, C., Tzankov, A., Zhang, J., Manyam, G. C., Xiao, M., Miao, Y., Jabbar, K., Tan, X., Pang, Y., Visco, C., Xie, Y., Dybkaer, K., Chiu, A., Orazi, A., Zu, Y., Bhagat, G., Richards, K. L., Hsi, E. D., Choi, W. W. L., van Krieken, J. H., Huh, J., Ponzoni, M., Ferreri, A. J. M., Møller, M. B., Parsons, B. M., Winter, J. N., Piris, M. A., Li, S., Miranda, R. N., Medeiros, L. J., Li, Y., Xu-Monette, Z. Y., & Young, K. H. (2018). Clinical Significance of PTEN Deletion, Mutation, and Loss of PTEN Expression in De Novo Diffuse Large B-Cell Lymphoma. *Neoplasia*, 20(6), 574–593. <https://doi.org/10.1016/j.neo.2018.03.002>
- Wang, Y., He, G., Wang, F., Zhang, C., Ge, Z., Zheng, X., & Tang, K. (2019). Aspirin inhibits adipogenesis of tendon stem cells and lipids accumulation in rat injury tendon through regulating PTEN/PI3K/AKT signalling. *Journal of Cellular and Molecular Medicine*, 23, 7535–7544. <https://doi.org/10.1111/jcmm.14622>
- Xi, Y., & Chen, Y. (2017). PTEN plays dual roles as a tumor suppressor in osteosarcoma Cells. *Journal of Cellular Biochemistry*, 118, 2684–2692. <https://doi.org/10.1002/jcb.25888>
- Yang, Z., Liu, Y., Shi, C., Zhang, Y., Lv, R., Zhang, R., Wang, Q., & Wang, Y. (2017). Suppression of PTEN/AKT signaling decreases the expression of TUBB3 and TOP2A with subsequent inhibition of cell growth and induction of apoptosis in human breast cancer MCF-7 cells via ATP and caspase-3 signaling pathways. *Oncology Reports*, 37, 1011–1019. <https://doi.org/10.3892/or.2017.5358>
- Yu, X., Chen, Y., Tian, R., Li, J., Li, H., Lv, T., & Yao, Q. (2017). miRNA-21 enhances chemoresistance to cisplatin in epithelial ovarian cancer by negatively regulating PTEN. *Oncology Letters*, 14, 1807–1810. <https://doi.org/10.3892/ol.2017.6324>
- Zhao, W., Han, T., Li, B., Ma, Q., Yang, P., & Li, H. (2019). miR-552 promotes ovarian cancer progression by regulating PTEN pathway. *Journal of Ovarian Research*, 12, 121. <https://doi.org/10.1186/s13048-019-0589-y>
- Zheng, C., Tang, F., Min, L., Hornicek, F., Duan, Z., & Tu, C. (2020). PTEN in osteosarcoma: Recent advances and the therapeutic potential. *Biochimica Et Biophysica Acta (BBA) - Reviews on Cancer*, 1874(2), 188405–<https://doi.org/10.1016/j.bbcan.2020.188405>
- Zhu, Y., Long, H. T., Zeng, L., Tang, Y. F., Zhao, R. B., Lin, Z. Y., & Cheng, L. (2019). MiR-19b-3p regulates osteogenic differentiation of PDGFRalpha(+) muscle cells by specifically targeting PTEN. *Cell Biology International*, 43, 565–573. <https://doi.org/10.1002/cbin.11133>

## SUPPORTING INFORMATION

Additional supporting information may be found in the online version of the article at the publisher's website.

**How to cite this article:** Nowwarote, N., Osathanon, T., Fournier, B. P. J., Theerapanon, T., Yodsanga, S., Kamolratanakul, P., Porntaveetus, T., & Shotelersuk, V. (2021). PTEN regulates proliferation and osteogenesis of dental pulp cells and adipogenesis of human adipose-derived stem cells. *Oral Diseases*, 00, 1–12. <https://doi.org/10.1111/odi.14030>